Supplementary Materials:

Aminoglycoside Activity Observed on Single Pre-translocation Ribosome Complexes

Michael B. Feldman[1,2], Daniel S. Terry[1,3], Roger B. Altman[1] & Scott C. Blanchard[1]*

[1]Department of Physiology and Biophysics, Weill Medical College of Cornell University,
[2] Weill Cornell / Rockefeller University / Sloan-Kettering Tri-Institutional MD-PhD Program,
[3]Tri-Institutional Training Program in Computational Biology and Medicine,
1300 York Avenue, New York, NY 10065, USA
**Correspondence: scb2005@med.cornell.edu*

Nature Chemical Biology: doi:10.1038/nchembio.274

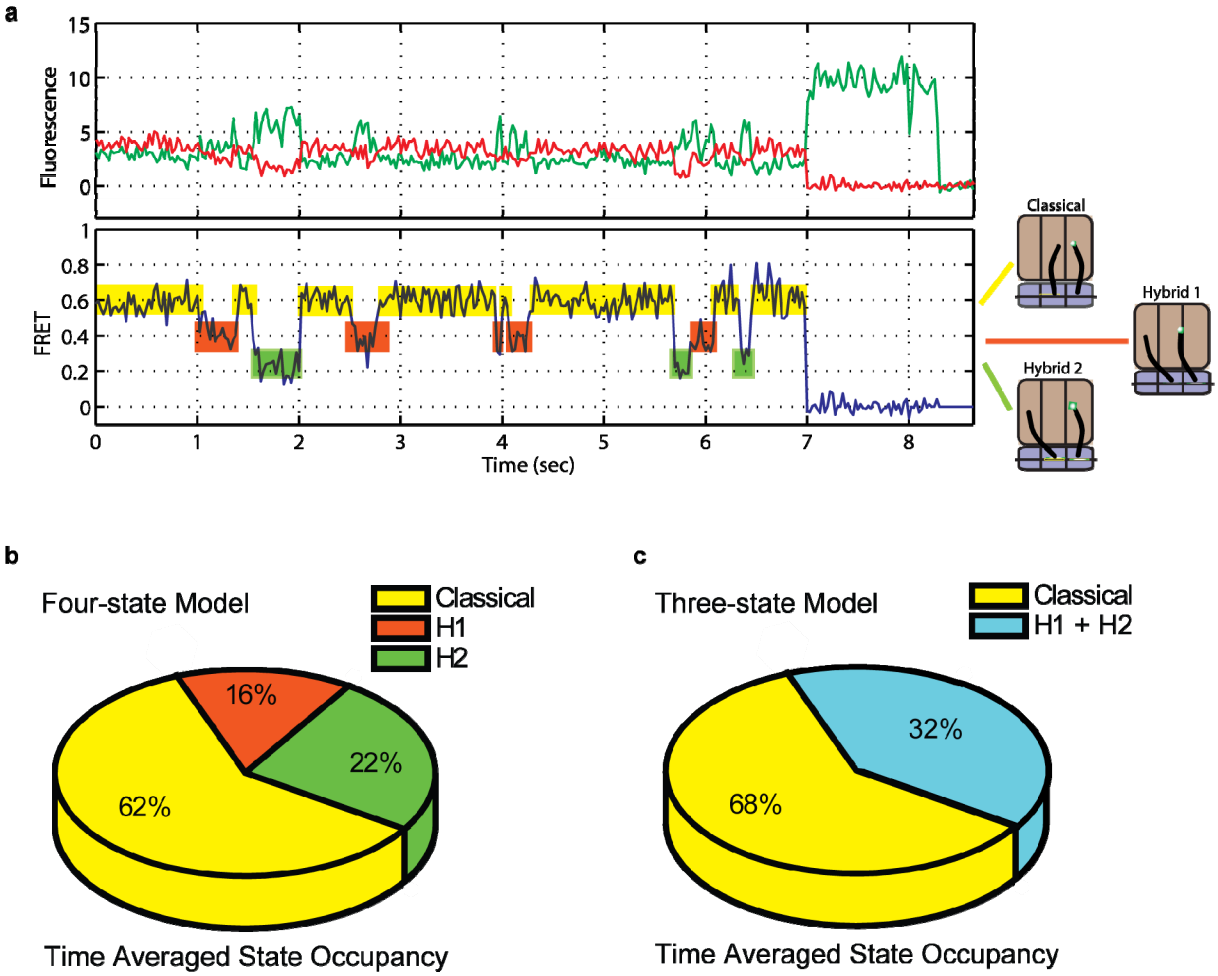

Supplementary Figure 1: Analysis of tRNA dynamics through smFRET measurements. Single-molecule fluorescence traces were collected and FRET was calculated according to the equation: $FRET=I_{Cy5}/(I_{Cy3}+I_{Cy5})$. (**a**) A representative single-molecule trace of tRNA-tRNA FRET in the wild type pre-translocation ribosome complex is shown. FRET traces were assigned to specific states using automated Hidden Markov Modeling algorithms (Methods). Here, dwells in a given state are represented by the individual segments of the FRET traces highlighted in yellow (Classical), red (Hybrid state-1; H1), and green (Hybrid state-2; H2). Dwells in the photobleached (0-FRET) state are not highlighted. (**b,c**) Time-averaged state occupancy, the fraction of time a population of ribosomes spends in a particular conformation, were calculated by adding the total dwell times spent in a particular state and dividing by the total time observed for all molecules in all non-zero FRET states. Time averaged state occupancies in both classical and hybrid states are shown for both the (**b**) four-state and (**c**) three-state models employed (Methods).

Nature Chemical Biology: doi:10.1038/nchembio.274

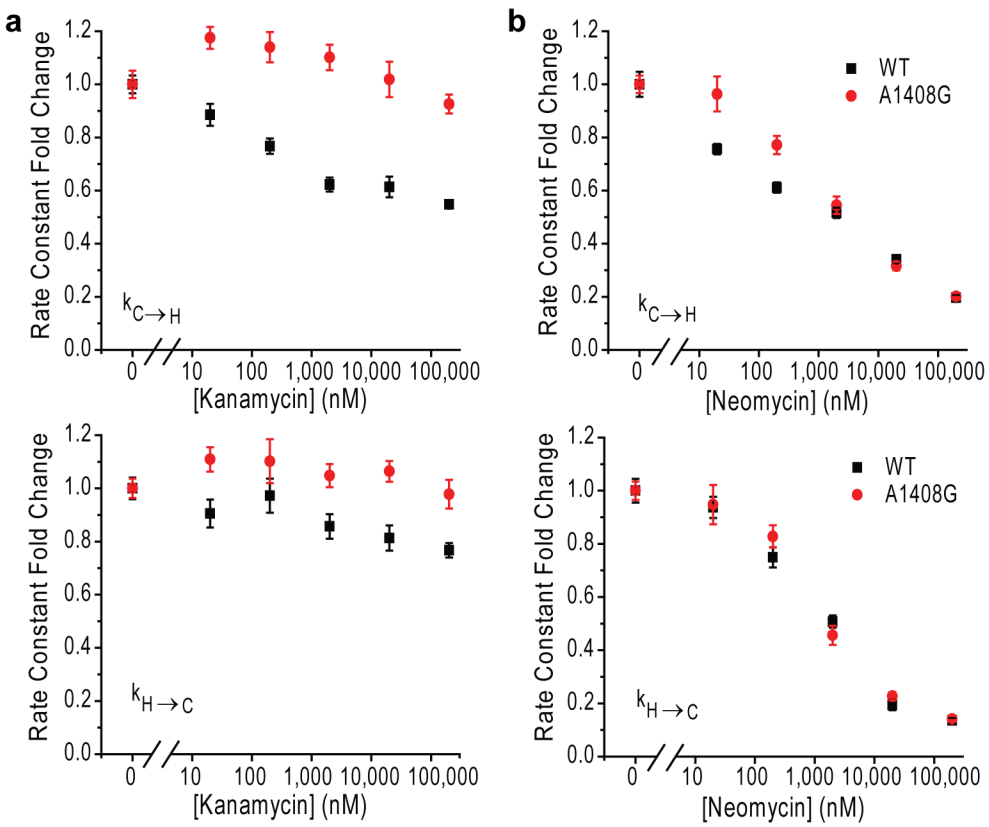

Supplementary Figure 2: Kanamycin and neomycin exhibit distinct effects on tRNA dynamics within the pre-translocation ribosome complex. Single-molecule FRET traces obtained from wild-type ribosomal complexes (black squares) and ribosomes containing the A1408G aminoglycoside resistance mutation (red circles) were idealized to a three-state model with one hybrid state and one classical state (Methods). Rate constants of specific transition types are shown with increasing concentrations of (**a**) kanamycin and (**b**) neomycin, relative to observations in the absence of drug. Error bars are standard error of the mean, as calculated using 10 bootstrap samples. (**a**) In the wild-type system, addition of kanamycin leads to a modest decrease in $k_{C\rightarrow H}$ (black squares, top panel) and a smaller decrease in $k_{H\rightarrow C}$ (black squares, bottom panel), consistent with kanamycin stabilizing the classical relative to hybrid states and reducing overall dynamics in the system. Such effects were generally not observed in pre-translocation complexes containing an A1408G aminoglycoside resistance mutation (red circles). (**b**) For the wild-type system, neomcyin at low concentrations (less than or equal to 20 nM) led to reductions in $k_{C\rightarrow H}$ (top panel) while $k_{H\rightarrow C}$ (bottom panel) was largely unchanged. Higher neomycin concentrations lead to dramatic reductions in both rates. In pre-translocation complexes containing an A1408G aminoglycoside resistance mutation, the low-concentration neomycin effects on $k_{C\rightarrow H}$ were substantially diminished, while those observed at higher concentrations remained. Error bars were calculated using bootstrapping (N=10).

Nature Chemical Biology: doi:10.1038/nchembio.274

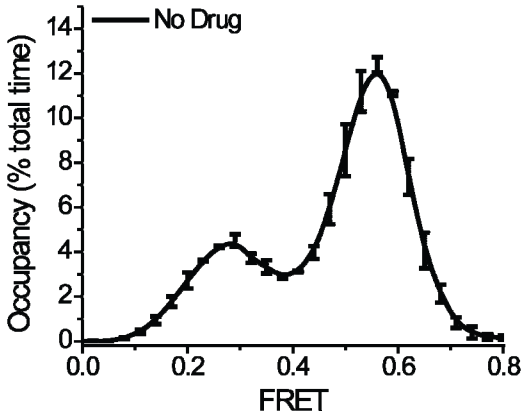

Supplementary Figure 3: Single-molecule FRET experiments are highly reproducible on a day-to-day basis. Time-averaged FRET state occupancy was measured in three independent experiments on three separate days for surface immobilized wild-type 70S E. coli ribosome complexes (see Supplementary Figure 1). Day-to-day variability was quantified by measuring time-averaged FRET state occupancy on three separate occasions over a two month period for wild-type ribosomes, where the mean ± standard deviation is shown. Experimental errors were estimated as the standard deviation at each point in the population FRET histogram. Day-to-day variability in time-averaged FRET state occupancies was ±3.0% (standard deviation).

Nature Chemical Biology: doi:10.1038/nchembio.274

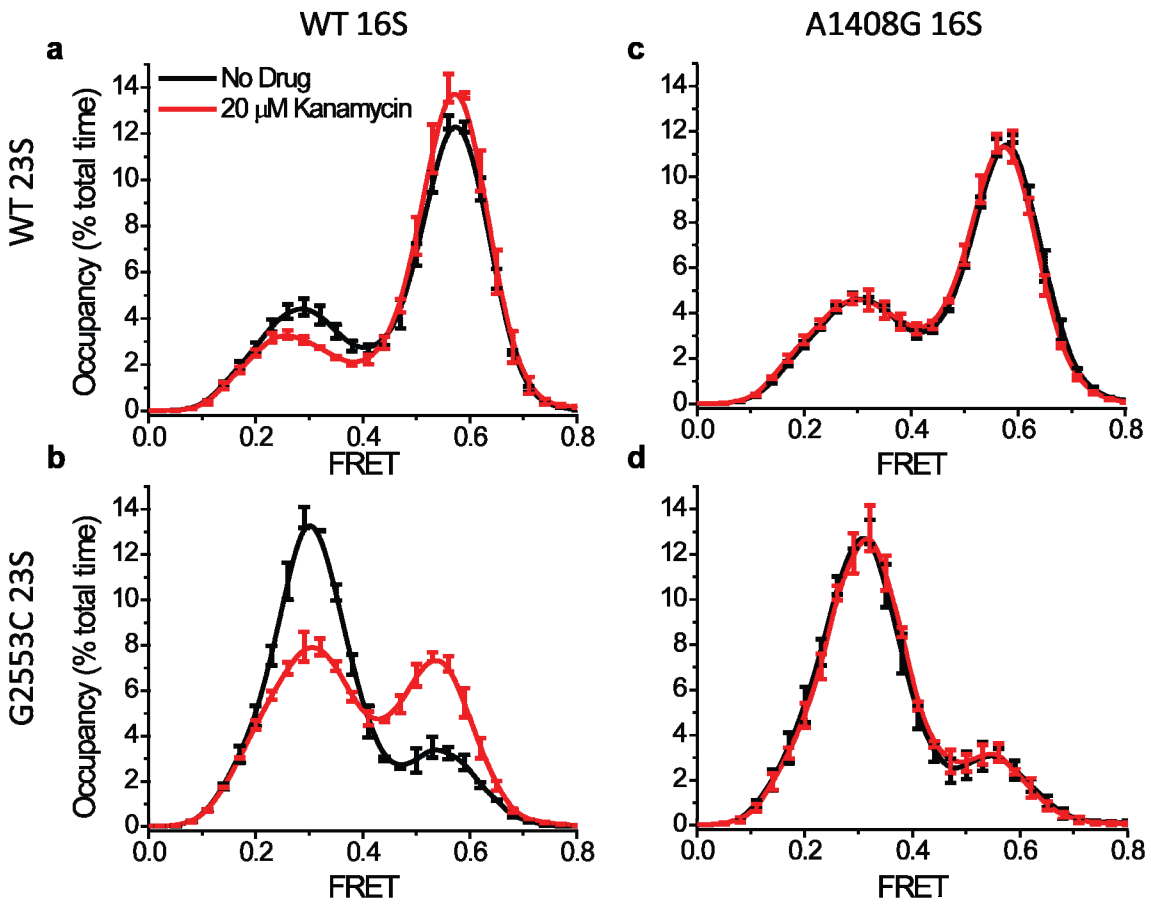

Supplementary Figure 4: Kanamycin-induced changes in FRET are highly reproducible on an experiment-to-experiment basis. Time-averaged FRET state occupancies measured in three independent experimental repeats performed on the same day were obtained for surface immobilized, wild-type ribosome complexes (Supplementary Figure 1). Experiment-to-experiment errors within a given day were measured in the absence of drugs (black lines) and presence of 20 µM kanamycin (red lines) for (**a**) wild-type, (**b**) G2553C 23S, (**c**) A1408G 16S, and (**d**) G2553C 23S + A1408G 16S ribosomal complexes. The mean ± standard deviation of FRET histograms from triplicate experiments is shown. In the case of wild-type 16S decoding site ribosome complexes (**a-b**), changes in classical state occupancy were significantly larger than the observed experimental error (p=0.046 for WT 23S and p=0.0021 for G2553 23S, calculated using two-sample *t* test). On average, experiment-to-experiment variability in time-averaged state occupancy was ±2.3% (standard deviation), with the exception of the G2553C 23S + 1408G 16S ribosomal complexes, which had larger errors (standard deviation = 5.4%) at least in part due to a small number of molecules in each experiment. To minimize the contribution of error to the experimental results, each titration and group of single molecule experiments presented in this study were performed from a common buffer stock on a single day.

Nature Chemical Biology: doi:10.1038/nchembio.274

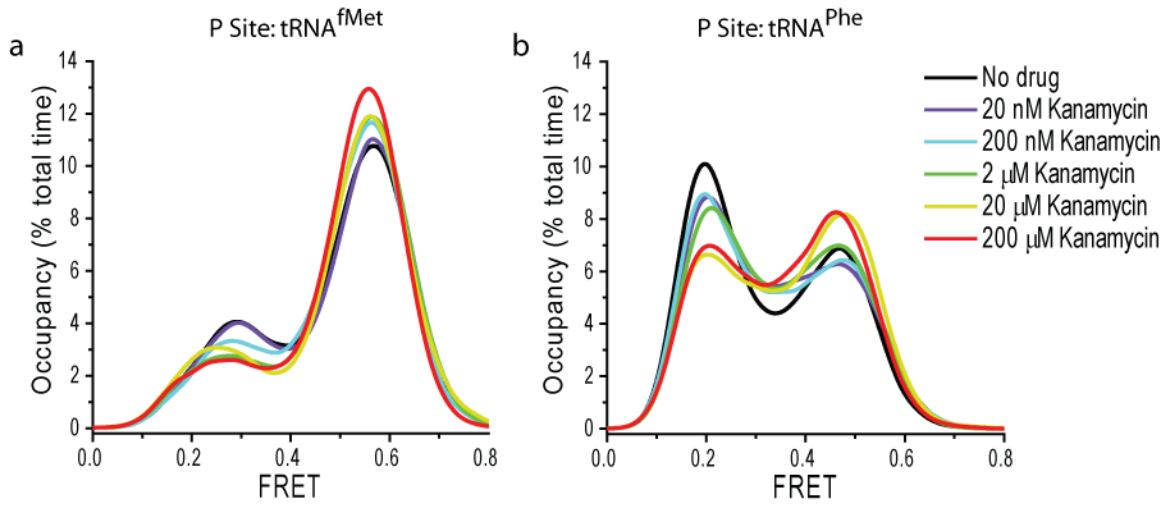

Supplementary Figure 5: Changes in FRET state occupancies observed in the presence of aminoglycosides were similar for distinct pre-translocation complexes. Ribosomal complexes containing either (**a**) P-site $tRNA^{fMet}$(Cy3-s^4U8) and A-site Phe-$tRNA^{Phe}$(Cy5-acp^3U47) or (**b**) P site Phe-$tRNA^{Phe}$(Cy3-s^4U8) and A site Lys-$tRNA^{Lys}$(Cy5-acp^3U47) were investigated using smFRET imaging. Time-averaged occupancy in FRET states is shown for increasing concentrations of kanamycin.

Nature Chemical Biology: doi:10.1038/nchembio.274

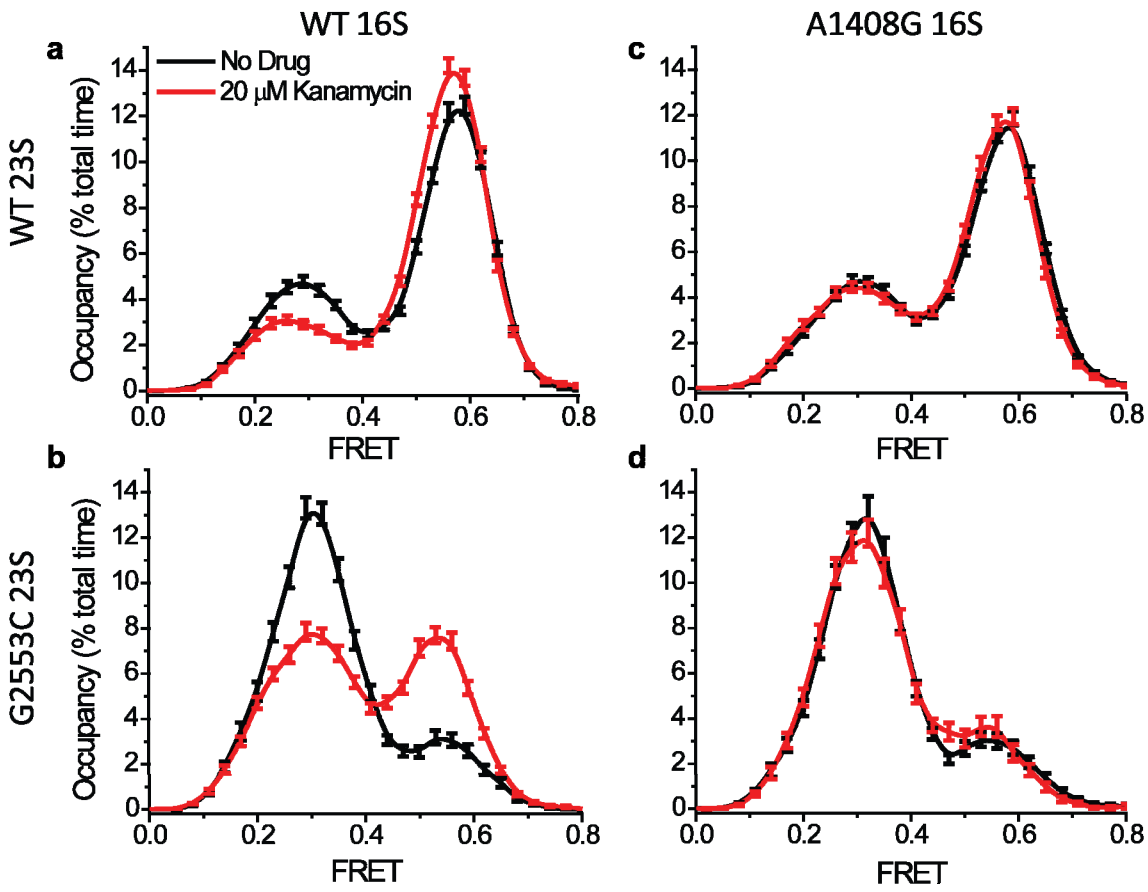

Supplementary Figure 6: Estimate of analytical error in smFRET measurements. The time-averaged occupancy in FRET states was measured for surface immobilized 70S E. coli ribosome complexes (see Supplementary Figure 1) in the absence of drugs (black lines) and in the presence of 20 μM kanamycin (red lines). Error in the FRET histograms, estimated as the standard deviation of 1,000 bootstrap samples, is used to approximate the experimental error, which is of a similar magnitude (Supplementary Figure 4). FRET distributions are shown for single experiments from the triplicate repeats described in Supplementary Fig. 4 for (**a**) wild-type, (**b**) G2553C 23S, (**c**) A1408G 16S, and (**d**) G2553C 23S + A1408G 16S ribosomal complexes. The high-FRET peak (~0.56) is consistent with the classical state and the lower-FRET peak (~0.3) is consistent with hybrid states. Wild-type 16S ribosomal complexes (**a,b**) show increased classical state occupancy that is significantly larger than the calculated errors. In contrast, the comparable A1408G 16S ribosomal complexes (**c,d**) show changes in the FRET distribution that often fall within calculated errors. The bootstrapped errors for the (**d**) G2553C 23S + A1408G 16S sample (±4.5%) were substantially larger than those observed for the other three datasets in a manner consistent with directly observed experimental errors (Supplementary Fig. 4).

Nature Chemical Biology: doi:10.1038/nchembio.274

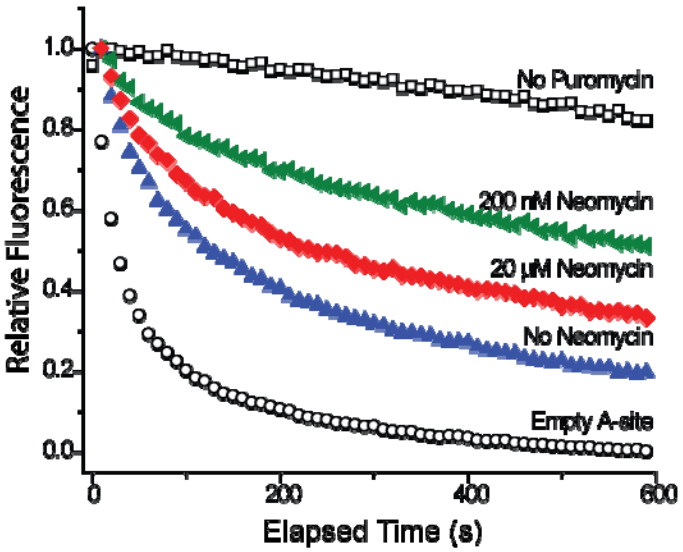

Supplementary Figure 7: The bimodal of nature neomycin binding to the pre-translocation complex is confirmed by puromycin reactivity experiments. Upon stopped-flow delivery of 20 µM puromycin, the loss of fluorescence observed in surface-immobilized pre-translocation complexes containing $tRNA^{fMet}$ in the P site and Cy3-DSP-Met-Phe-$tRNA^{Phe}$ in the A site reports on neomycin-induced changes in the exchange between classical and hybrid tRNA configurations (Methods). Classical peptidyl-tRNA configurations do not react appreciably with puromycin, while hybrid configurations, by placing peptidyl-tRNA in the P site, react rapidly with puromycin. Reaction rates are shown relative to photobleaching rates (no puromycin) and experiments in which peptidyl-tRNA occupies the P site. Residual puromycin reactivity observed in the pre-translocation complex in the absence of neomycin reports on time-averaged hybrid state occupancy. At 200 nM neomycin, puromycin reactivity is reduced relative to the pre-translocation complex, consistent with increased classical state occupancy. At 20 µM neomycin, puromycin reactivity is partially restored, consistent with increased hybrid state occupancy.

Nature Chemical Biology: doi:10.1038/nchembio.274

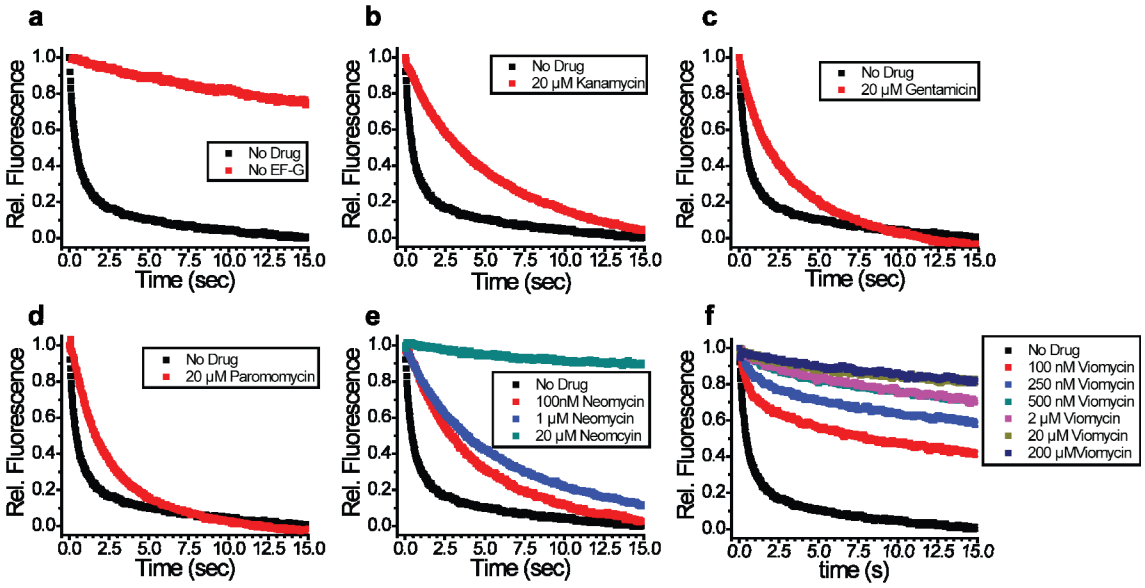

Supplementary Figure 8: Structurally-distinct aminoglycosides inhibit translocation to different extents. Single-step EF-G-dependent translocation rates were measured for wild-type ribosomes containing $tRNA^{fMet}$ in the P site and fMet-Phe-$tRNA^{Phe}$ in the A site in the presence and absence of specific aminoglycoside antibiotics using a previously established method[1] (Methods). The decay of pyrene fluorescence was fit to a double exponential where the dominant, fast component reports on the rate of factor-dependent translocation. (**a**) Fluorescence decay is minimal in the absence of EF-G (**b**) kanamycin concentrations (20 µM) that strongly stabilize classical state occupancy show large reductions in translocation rates. Gentamicin (**c**) and paromomycin (**d**), which provide less classical state stabilization, show diminished levels of translocation inhibition. At 100 nM neomycin (**e**), similar levels of translocation inhibition are observed. At 20 µM neomycin, where hybrid state occupancy is promoted and transition rates are significantly reduced, almost complete inhibition of translocation is observed. Viomycin (**f**) reduces both the rate and extent of translocation suggesting a distinct mechanism of translocation inhibition from aminoglycoside antibiotics. At 20µM, neomycin and viomycin had similar affects on the rate and extent of translocation. Translocation rates are reported in Supplementary Table 3.

Nature Chemical Biology: doi:10.1038/nchembio.274

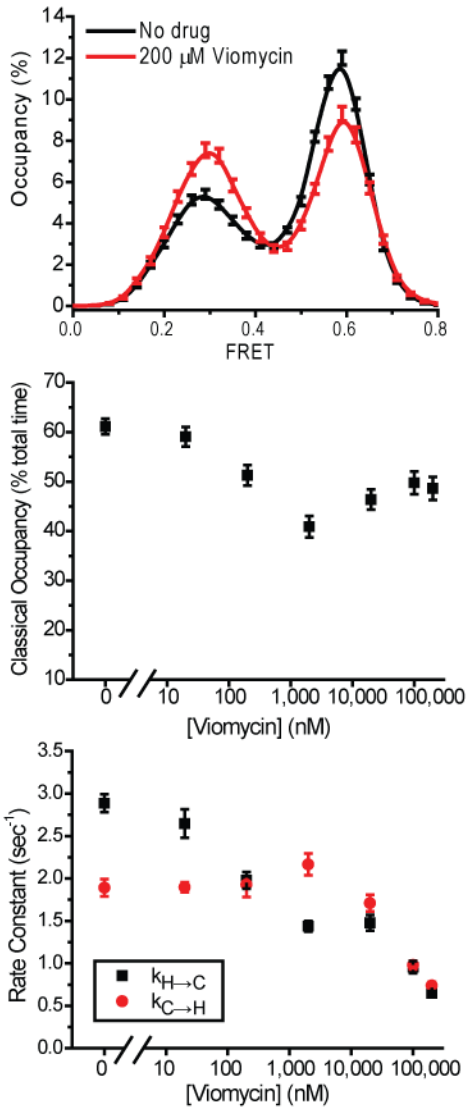

Supplementary Figure 9: Viomycin preferentially stabilizes distinct states depending on drug concentrations. (Top panel) The time-averaged distribution of FRET values in all non-zero FRET states is shown in the absence of drugs (black line) and in the presence of 200 μM viomycin (red line). Single-molecule FRET trajectories from experiments performed in the presence of increasing viomycin concentrations were idealized to a 3-state hidden Markov model (Methods). (Middle panel) Time-averaged occupancy in the classical tRNA configuration and (bottom panel) maximum likelihood estimates are shown of rate constants of transition from classical to hybrid states ($k_{C\rightarrow H}$, red circles) and hybrid to classical states ($k_{H\rightarrow C}$, black squares).

Nature Chemical Biology: doi:10.1038/nchembio.274

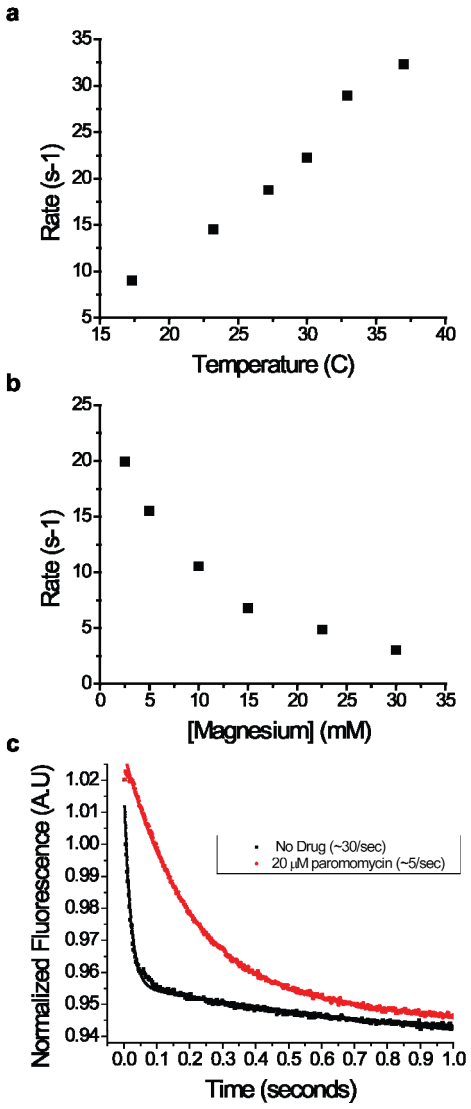

Supplementary Figure 10: Experimental temperature and buffer conditions have predictable effects on translocation. Single-step EFG-dependent translocation rates were measured for wild-type ribosomes containing $tRNA^{fMet}$ in the P site and fMet-Phe-$tRNA^{Phe}$ in the A site (Supplementary Methods) in the presence of 2.5 µM EF-G and 1 mM GTP. The average rates of experiments performed in triplicate are shown where the standard deviation in these values are ± 7%. (a) The translocation rates of BL21 ribosomes were measured at 5 mM magnesium over a range of temperatures. (b) The translocation rates of BL21 ribosomes were measured at 25°C over a range of magnesium ion concentrations. (c) Single-step EFG-dependent translocation rates were also measured for wild-type BL21 pre-translocation complexes in the absence and presence of 20 µM paromomycin at 37°C in polymix buffer (pH 7.5) containing 5 mM magnesium. The average rates of experiments performed in triplicate are shown: ~$30sec^{-1}$ and ~$5sec^{-1}$ in the absence and presence of drug.

Nature Chemical Biology: doi:10.1038/nchembio.274

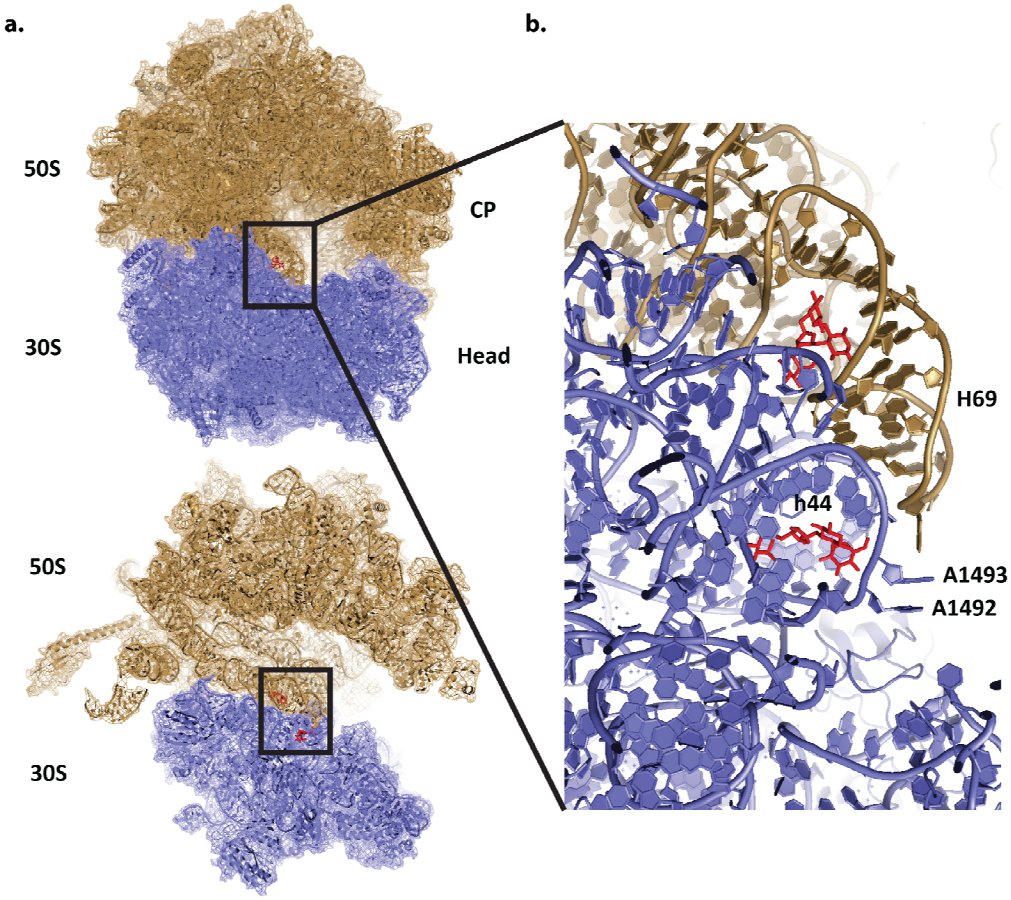

Supplementary Figure 11: Neomycin binds two functionally distinct binding sites on the 70S ribosome. The 70S ribosome (PDB accession codes: 2QAN and 2QAO1)[2] is shown oriented such that the E-site faces out of the page and the central protuberance (CP) and the head region (Head) project to the right to allow visualization of the aminoglycoside binding sites (**a, top**), and oriented with a 90° clockwise rotation around a vertical axis such that the A-, P-, and E-sites can be observed with the CP and Head removed (**a, bottom**). An enlarged view of the neomycin binding regions observed on h44 and H69 is provided (**b**). Neomycin (red) is shown bound to the 30s ribosomal subunit (blue) within the canonical h44 decoding site where the 16S rRNA residues A1492 and A1493 are observed to be extruded from the helix. Neomycin is also shown bound to the 50S ribosomal subunit (tan) within H69 of 23S rRNA.

Nature Chemical Biology: doi:10.1038/nchembio.274

Supplementary Table 1:

Apparent Transition Rate Constants (s^{-1})						
	$k_{C\rightarrow H1}$	$K_{H1\rightarrow C}$	$K_{H1\rightarrow H2}$	$K_{H2\rightarrow H1}$	$k_{C\rightarrow H2}$	$K_{H2\rightarrow C}$
WT 23S + WT 16S						
No Drug	1.34±0.25	5.54 ±0.25	1.70 ±0.09	1.43 ±0.09	1.02 ±0.05	2.38 ±0.13
200 μM	0.48 ±0.02	2.92 ±0.22	1.05 ±0.07	0.71 ±0.06	0.76 ±0.03	2.24 ±0.16
WT 23S + A1408G 16S						
No Drug	1.05 ±0.05	4.76 ±0.11	1.51 ±0.14	0.87 ±0.05	0.94 ±0.06	2.01 ±0.13
200 μM	1.20 ±0.05	4.25 ±0.18	1.50 ±0.07	1.34 ±0.08	0.76 ±0.04	2.24 ±0.11
G2553C 23S + WT 16S						
No Drug	3.00 ±0.24	1.25 ±0.13	0.94 ±0.06	1.18 ±0.07	0.49 ±0.04	0.24 ±0.05
200 μM	2.16 ±0.07	3.50 ±0.25	1.41 ±0.07	1.60 ±0.07	0.40 ±0.03	0.51 ±0.06
G2553C 23S + A1408G 16S						
No Drug	2.47 ±0.22	0.54 ±0.03	1.02 ±0.06	1.21 ±0.06	0.87 ±0.07	0.25 ±0.02
200 μM	3.17 ±0.20	1.34 ±0.11	1.07 ±0.08	1.38 ±0.09	0.68 ±0.05	0.41 ±0.05

Kanamycin changes the rate constants governing A-site and P-site tRNA motion. Rate constants governing tRNA hybrid state formation were calculated using an automated Maximum-Interval Likelihood algorithm for the four-state model (Methods), and are reported ±standard error of the mean (SEM). Standard errors were calculated as the standard deviation of rate constants estimated from 10 bootstrap samples (Methods). Analysis of experimental replicates for a limited number of samples yielded a standard deviation of ±0.2 s^{-1}. Errors observed for the G2553C 23S + A1408G 16S in experimental replicates were substantially larger than those observed for the other three samples (standard deviation = 0.5 s^{-1}).

Nature Chemical Biology: doi:10.1038/nchembio.274

Supplementary Table 2:

Ground State Energy (ΔΔG) of Classical State (kJ mol^{-1})			
	Relative to H1	**Relative to H2**	**Relative to H1+H2**
WT			
No Drug	-3.43 ±0.01	-2.64 ±0.02	-1.72 ±0.02
200 μM	-4.43 ±0.01	-3.26 ±0.02	-2.41 ±0.02
Δ	-1.00 ±0.01	-0.62 ±0.03	-0.69 ±0.03
A1408G 16S			
No Drug	-3.71 ±0.02	-2.31 ±0.03	-1.59 ±0.03
200 μM	-3.20 ±0.02	-2.92 ±0.02	-1.72 ±0.02
Δ	0.51 ±0.03	-0.61 ±0.04	-0.13 ±0.04
G2553C 23S			
No Drug	1.99 ±0.31	1.60 ±0.27	2.76 ±0.35
200 μM	-1.22 ±0.05	-1.43 ±0.05	-0.38 ±0.06
Δ	-3.21 ±0.31	-3.03 ±0.27	-3.14 ±0.36
G2553C 23S + A1408G 16S			
No Drug	3.36 ±0.92	4.45 ±1.34	4.35 ±0.77
200 μM	1.32 ±0.28	1.99 ±0.35	2.68 ±0.24
Δ	-2.04 ±0.96	-2.46 ±1.38	-1.67 ±0.81

Kanamycin stabilizes classical tRNA configurations. Ground state energies (ΔG) of the classical state relative to either the hybrid 1 (H1) or hybrid 2 (H2) state, or combined H1+H2 occupancy, were calculated from the state occupancies (Methods). Assignment of classical, H1, and H2 state occupancies was performed using the four-state model, while assignment of occupancies for the H1+H2 state was performed using the three-state model. Errors were propagated from the SEM measured from state occupancy.

Nature Chemical Biology: doi:10.1038/nchembio.274

Supplementary Table 3:

4,5- and 4,6-linked Aminoglycosides			
	Classical State Occupancy (% total time)	Global Transition Rate (t/s)	Translocation Rate (s^{-1})
No Drug	62.4 ± 1.1	2.67 ± 0.07	1.57 ± 0.05
Kanamycin	69.6 ± 1.0	1.90 ± 0.04	0.27 ± 0.02
Neomycin (100 nM)	70.3 ± 1.9	2.45 ± 0.12	0.31 ± 0.05
Neomycin (20 μM)	52.0 ± 1.5	0.97 ± 0.03	0.06 ± 0.01
Gentamicin	67.2 ± 0.9	2.26 ± 0.05	0.42 ± 0.04
Paromomycin	63.9 ± 1.3	1.80 ± 0.05	0.51 ± 0.06
Other Compounds			
Viomycin (200 μM)	46.8 ± 2.4	1.09 ± 0.05	0.04 ± 0.01

The association of classical state stabilization and translocation inhibition is governed by a monotonic relationship for decoding site binding aminoglycosides. Classical state occupancy (% total time; assigned using the four-state model), global transition rates (t/s; number of state transitions per molecule per second) and single-step factor-dependent translocation rates (s^{-1} ± SD) are shown for aminoglycoside antibiotics known to bind in the small subunit decoding site, as well as for other compounds that alter ribosome function. Error in translocation rates was calculated from three repeat experiments. Among the decoding site binding aminoglycosides, there is a monotonic relationship between classical state occupancy and translocation rate, with the exception of 20μM neomycin. The translocation rates measured for 20 μM neomycin and 200 μM viomycin were similar in magnitude to the no EF-G control (Supplementary Fig. 8).

Nature Chemical Biology: doi:10.1038/nchembio.274

Supplementary Methods

Measurement of puromycin reactivity

Puromycin reactivity, reporting on peptidyl-tRNA occupancy in the P site was measured as previously described[3] in 20 mM puromycin at pH 7.5. Puromycin reacts with peptidyl tRNA in the PTC, where the Cy3-labeled nascent peptide is transferred to the puromycin followed by rapid dissociation from the ribosome and diffusion out of the imaging plane.

Measurement of bulk single-step translocation rates on the ribosome

Initiation complexes were prepared *in vitro* by incubating ribosomes (3 μM) isolated from *E. coli* strain BL21(DE3)* (Invitrogen) with pyrene-labeled mRNA (6 μM), IF-1, IF-2, IF-3 (4 μM each), phosphoenolpyruvate (300 μM), pyruvate kinase (3.7 μg/ml), myokinase (7 μg/ml) and ribosomal protein S1 (3 μM), with 2 mM GTP and 4 μM fMet-tRNA^{fMet} in Tris-polymix buffer containing 5 mM $Mg(OAc)_2$. Pre-translocation complexes were prepared by incubating initiation complexes (2 μM) with the ternary complex of EF-Tu(GTP)phe-tRNA^{Phe} (4 μM) for 5 min at 37°C in Tris-polymix buffer containing 5 mM $Mg(OAc)_2$ and purified by pelleting through a 1.1 M sucrose cushion prepared with Tris-polymix buffer and 15 mM $Mg(OAc)_2$ at 80,000xg for 2 hours followed by resuspension in the same buffer. Rapid translocation experiments were performed on a SC.180MV-R stopped-flow fluorimeter (Applied Photophysics) where pre-translocation ribosome complexes (200 nM) were rapidly mixed with 5 μM EF-G and 1 mM GTP in Tris-polymix buffer containing 15 mM $Mg(OAc)_2$ at 23°C to final concentrations of 100 nM ribosome complexes, 2.5 μM EF-G, and 500 μM GTP. Buffer conditions were chosen so as to maintain consistency with the single molecule experiments. Antibiotics were added to both the initiation complex and EF-G/GTP solutions prior to mixing.

Fluorescence decay was monitored using λ_{ex} = 343 nm (bandwidth = 2 nm) and a 375-nm cut-off filter (Semrock FF01-377/50-25) for fluorescence emission. Individual results were fit to a double exponential decay function, with the fast component reporting the rate of single-step mRNA-tRNA translocation (ProData Viewer). In all experiments, the slow component was similar to the single-exponential decay ($k \approx 0.04$ sec^{-1}) observed in the presence of 200 μM viomycin, and that observed in the absence of EF-G.

Experimental and analytical error analysis

The reproducibility and estimated experimental error in the smFRET measurement were examined by performing subsets of the panel of experiments shown in Figure 1 in triplicate. These independent experiments demonstrated that FRET state occupancies could be reproducibly determined with a standard deviation of 2.3% (**Supplementary Fig. 4**). All comparative titration experiments were performed on the same day in order to minimize the slightly greater day-to-day variability (3% standard deviation) of the experiment (**Supplementary Fig. 3**). Unless otherwise stated, error estimates were assessed using bootstrap analysis, which closely approximated the aforementioned experimental errors (**Supplementary Fig. 6**). Here, FRET state occupancies are reported as standard errors (±1.5% with the exception of experiments performed in the G2553C 23S + A1408G 16S mutant background, where the

Nature Chemical Biology: doi:10.1038/nchembio.274

standard deviation was 4.5%). Expected errors at each point in FRET histograms were estimated as the standard deviation over 1,000 bootstrap samples, each generated by randomly selecting traces with replacement. Expected errors in time-averaged state occupancies and average transition rates were estimated as the standard deviation across 1,000 bootstrap samples of idealized smFRET traces. Standard errors in rate constant estimates were obtained as the standard deviation of rate constants over 10 bootstrap samples obtained from the maximum interval likelihood method[4].

Supplemental References

1. Studer, S. M., Feinberg, J. S. & Joseph, S. Rapid kinetic analysis of EF-G-dependent mRNA translocation in the ribosome. J Mol Biol 327, 369-81 (2003).
2. Borovinskaya, M. A. et al. Structural basis for aminoglycoside inhibition of bacterial ribosome recycling. Nat Struct Mol Biol 14, 727-32 (2007).
3. Munro, J. B., Altman, R. B., O'Connor, N. & Blanchard, S. C. Identification of two distinct hybrid state intermediates on the ribosome. Mol Cell 25, 505-17 (2007).
4. Qin, F. Principles of single-channel kinetic analysis. Methods Mol Biol 403, 253-86 (2007).

Nature Chemical Biology: doi:10.1038/nchembio.274